Design of the enzyme-carrier interface to overcome the O_2 and NADH mass transfer limitations of an immobilized flavin-oxidase

Ana I. Benítez-Mateos,[†,‡,Ψ] *Christina Huber*[§] *Bernd Nidetzky,*[§,⊥] *Juan M. Bolivar,*[§,ς]* *and Fernando López-Gallego*[†,‡,ϒ,]*

[†] Center for Cooperative Research in Biomaterials (CIC biomaGUNE), Basque Research and Technology Alliance (BRTA), Paseo de Miramon 182, 20014, Donostia San Sebastián, Spain

[‡] Instituto de Síntesis Química y Catálisis Homogénea (ISQCH), CSIC-Universidad de Zaragoza, C/Pedro Cerbuna 12, 50009 Zaragoza, Spain

[Ψ] Department of Chemistry and Biochemistry, University of Bern, Freiestrasse3, 3012 Bern, Switzerland

[§] Institute of Biotechnology and Biochemical Engineering, Graz University of Technology, NAWI Graz, Petersgasse 12, A-8010 Graz, Austria

[⊥] Austrian Centre of Industrial Biotechnology, Krenngasse 37 , A-8010 Graz, Austria

[ς] Department of Chemical and Materials Engineering, Complutense University of Madrid, Madrid, Spain

[ϒ]Ikerbasque, Basque Foundation for Science, Maria Diaz de Haro 3, 48013 Bilbao, Spain

KEYWORDS: immobilized enzymes, substrate diffusion, O_2-sensing, mass transfer limitations, single-particle analysis.

ABSTRACT

Understanding how the immobilization of enzymes on solid carriers affects their performance is paramount for the design of highly efficient heterogeneous biocatalysts. Efficient supply of substrates onto the solid phase is one of the main challenges to maximize the activity of the immobilized enzymes. Herein, we apply advanced single-particle analysis to decipher the optimal design of an immobilized NADH oxidase (NOX) whose activity depends both on O_2 and NADH concentrations. Carrier physicochemical properties and its functionality, along with the enzyme distribution across the carrier were implemented as design variables to study the effects of the intraparticle concentration of substrates (O_2 and NADH) on the activity. Intraparticle O_2-sensing analysis revealed the superior performance of the enzyme immobilized at the outer surface in terms of effective supply of O_2. Furthermore, the co-immobilization of NADH and NOX within the tuned surface of porous microbeads increases the effective concentration of NADH in the surroundings of the enzyme. As result, the optimal spatial organization of NOX and its confinement with NADH allows to recover 100% of the activity of the soluble enzyme upon the immobilization process. By engineering these variables, we increase the NADH oxidation activity of the heterogeneous biocatalyst up to 650% compared to NOX immobilized under sub-optimal conditions. In conclusion, this work highlights the rational design and engineering of the enzyme-carrier interface to maximize the efficiency of heterogenous biocatalysts.

INTRODUCTION

Enzyme immobilization is a key enabling technology in synthetic, analytical and environmental chemistry. The binding of enzymes to solid materials eases the reaction control and sometimes stabilizes the resulting heterogeneous biocatalyst. Such stabilization allows the continuous and discontinuous utilization of enzymes for long operation times.[1,2] The functionality of immobilized enzymes inside solid matrix relies on spatiotemporal phenomena at nano-, micro- and macro-scale.[3–5] For example activity can be decreased by structural distortions and/or poor accessibility of the substrates to the enzyme active center (nanoscale), by limited substrate transport from the bulk to the material surface which creates intraparticle gradients of the reaction components (microscale),[4,6–9] and by sub-optimal reactor settings, like poor agitation (macroscale).

Particularly, the influence of the mass transport resistances and the resulting spatiotemporal gradients of reactants mainly depend on the carrier material characteristics (physico-chemical nature and internal architecture) and the catalyst localization inside the solid matrix.[10–12] In heterogeneous biocatalysis, like in heterogeneous chemical catalysis, porous carriers are preferred since their higher specific area enables to prepare catalysts with high volumetric activity.[13,14] In porous materials, the bound enzymes might suffer from both external mass transfer issues and internal diffusion restrictions, limiting the productivity of the heterogeneous biocatalysts. Traditionally, these mass transport issues are usually mitigated by decreasing the maximum reaction rate working at low enzyme loads (thus, sacrificing productivity), tuning carrier dimensions (particle and pore sizes) and the reactor configuration (fluid dynamics of mixing).[14,15] Additionally, the position of the enzymes within the carrier microstructure has also proven crucial to intensify the effectiveness of the heterogeneous biocatalysts,[16] since intraparticle enzyme distribution affects how substrate mass transfer impacts on the overall catalytic rate. For example glycosidases and acylases non-uniformly immobilized at the outer surface of porous microbeads overpower those uniformly distributed across the inner material porous surface.[17–23]

In the last years, our groups have proven to control the intraparticle protein distributions by altering the immobilization rates through tuning the chemical nature of the enzyme-carrier interface.[16,24] In this approach, a slow immobilization process allows enzymes to diffuse within the pores and colonize the entire 3D surface of the carriers, while rapid immobilization precludes the intraparticle diffusion of the enzyme, locating them at the outer shell of the porous particles.

To exert control over the immobilization rate, the immobilization chemistry plays a fundamental role since it defines the kinetics of the enzyme-carrier interactions. In previous studies, we found that the type and the density of reactive groups, as well as the immobilization conditions (temperature, pH, inhibitors…) determine the immobilization rate, and thus the position of the enzymes across the microstructure of the carriers. Although enzyme localization may be inferred from indirect studies that measure the catalytic activity in bulk experiments,[20] the use of specific dyes and advances in fluorescence-based microscopy have enabled to unambiguously reveal the enzymes spatial distribution, and correlate it with their intraparticle specific performance through luminophores sensitive to the reaction conditions (pH, oxygen, redox environment…).[25]

There are multiple examples where mass transfer effects are critical for catalyst efficiency. For instance, the process implementation of NAD(P)H flavin-oxidases (NOX) poses some difficulties. This family of enzymes is often exploited as cofactor recycling partner in NAD^+-dependent oxidation reactions, where substrates concentrations are rather low due to the poor water solubility of the oxygen and process imposed sub-stoichiometric amounts of the nicotinamide cofactors.[26,27] Moreover, NOX especially requires exogeneous FAD as redox mediator[28] and O_2 as electron acceptor to oxidize the NADH to NAD^+, producing H_2O_2 as side product, and consequently *in situ* recycling the pool of the oxidized cofactor. Otherwise the oxidase activity is too low for practical purposes. In this scenario, the low concentration of oxygen, NADH and FAD limit the NOX activity,[29–32] an issue that turns out dramatic when enzymes are immobilized on porous materials as these substrates and redox mediators must diffuse from the bulk (liquid) to the biocatalyst (solid-phase). The intraparticle O_2 depletion has been identified as one of the bottlenecks to intensify biotransformations driven by oxidases.[33–36] On the other hand, increasing the substrate concentration is not an option for high-cost molecules like NADH which high concentration during the biotransformation are undesired for the sake of the process economics. While O_2 and NADH limitations could be alleviated by application traditional approaches mentioned above, the engineering of the spatial distribution of the immobilized enzymes and their confinement with their limiting substrates (NADH) and redox mediators (FAD) are approaches never intended before to mitigate the diffusion restrictions underlying these enzymes.

In this work, we aim at designing an immobilized NOX from *Thermus thermophilus* HB27[37], through an integrative manner that involves the control of the enzyme localization, the tuning of material physico-chemical properties and the use of advanced internal sensing, to

ultimately mitigate the diffusion restrictions underlying this enzyme. To that end, we have prepared a battery of heterogeneous biocatalysts with different enzyme spatial organization within different porous materials, and further tested them under different mixing conditions. Evaluating all these influential parameters, we enhance 6.5-fold the catalytic performance of the best heterogeneous biocatalyst, reaching an immobilization effectiveness close to one, which means that its specific activity was close to the one reported for the free enzyme.

RESULTS AND DISCUSSION

Effect of NOX spatial organization on the activity of the immobilized biocatalyst. NOX was immobilized through aldehyde chemistry as previous results from our groups have proven to significantly stabilize NOX.[28] We used two classical carriers activated with glyoxyl (short-arm aliphatic aldehyde) groups but differing in their physico-chemical properties. One carrier is based on hydrophilic porous 6% agarose beads (AG-G) with a particle size of 50-150 μm and average pore size of 112 nm,[38] while the other is based on hydrophobic porous methacrylate beads (PU-G) with both larger particle (100-300 μm) and average pore (150 nm) sizes than the agarose ones. Using both carriers, NOX was quantitatively immobilized in 30 minutes under alkaline conditions driven by the nucleophilic attack of the ε-NH_2 groups of Lys in NOX surface, to the aldehydes of the carrier (Figure 1). These reactions formed reversible imines that were further reduced to the corresponding amine groups to make the enzyme attachment irreversible (Figure 1a). SDS-PAGE analysis reveals that the enzyme was irreversible attached to the carrier as no protein was detected after incubating the immobilized enzymes under denaturing conditions (Figure S1).

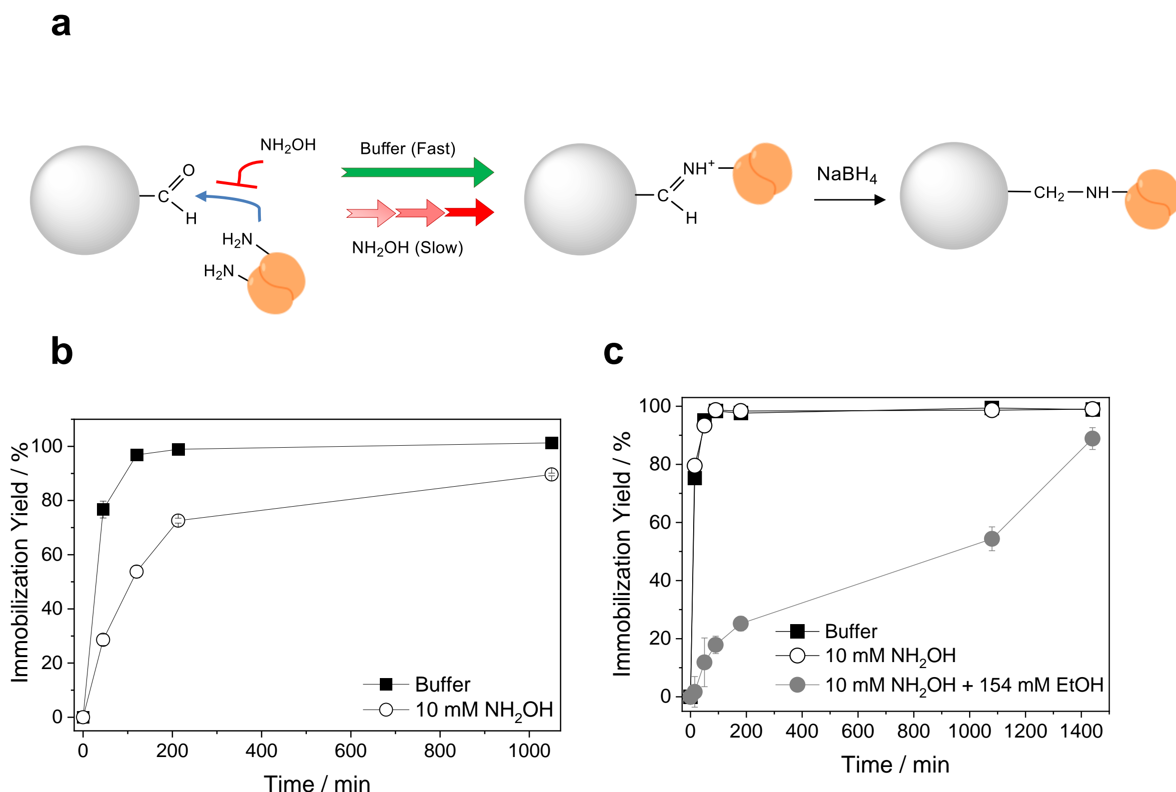

Figure 1. (a) Scheme of the NOX immobilization on carriers activated with aldehyde groups. NOX immobilization kinetics using (b) AG-G and (c) PU-G as porous carriers under different conditions. Enzyme load: 1 mg/g. Immobilization buffer: 100 mM sodium bicarbonate at pH 10.05.

Confocal laser scanning microscopy (CLSM) studies confirmed that NOX was mainly immobilized at the outer surface of both types of porous particles, according to previous results (Figure 2).[19,20,22–24] To study the effect of the spatial distribution on the performance of immobilized NOX, we immobilized this enzyme in presence of small molecules as immobilization competitors. According to this, Figure 1b shows how the presence of hydroxylamine (NH_2OH) reduces the immobilization rate of NOX on AG-G. The lower immobilization rate resulted in a supported biocatalyst where NOX was uniformly distributed across the porous surface of the carrier (Figure 2a). NH_2OH is highly reactive with aldehydes, and thus slows down the immobilization through competing with the Lys residues of NOX. The use of immobilization competitors was previously reported to control the spatial organization of His-tagged enzymes on carriers activated with metal chelates.[16]

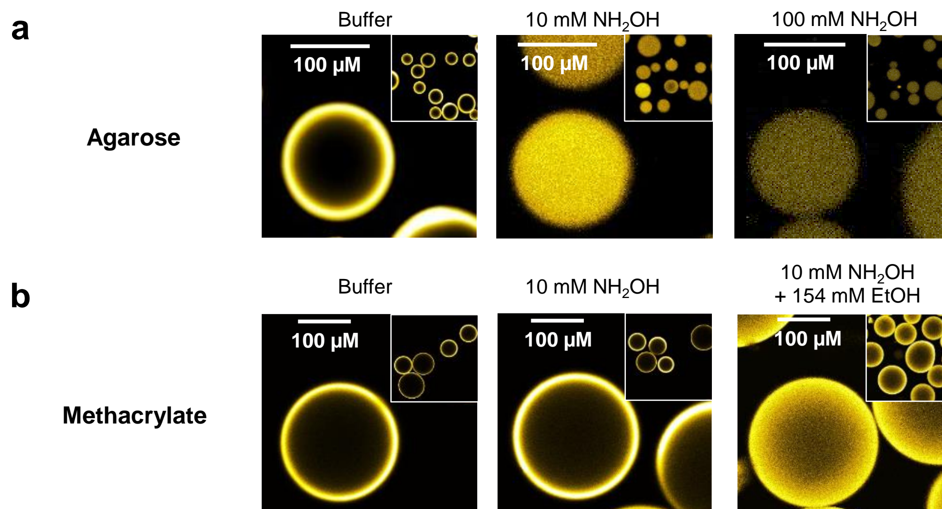

Figure 2. Spatial distribution of NOX immobilized on (a) agarose (AG-G) and (b) methacrylate (PU-G) microbeads under conditions described on the top of the micrographs. Autofluorescence of intrinsically FAD bound to resting NOX was harnessed to image the protein distribution. Images were analyzed by using FIJI (software for image analytics). A yellow hot LUT (Lookup Table for color grading) of the fluorescence signal is depicted.

Unfortunately, NH_2OH by itself was unable to slow down the immobilization of NOX on PU-G (Figure 1c). Such failure was manifested in the CLSM images (Figure 2b) where the spatial distribution of NOX was the same regardless the presence of NH_2OH during the immobilization process. The hydrophobic nature of the methacrylate materials may explain the inability of immobilization competitors to control the spatial organization of NOX. While the enzyme immobilization on AG-G is mainly driven by the aldehyde chemistry, PU-G can promote unspecific hydrophobic interactions that rapidly immobilize NOX even in presence of NH_2OH. We demonstrated such unwanted hydrophobic interactions by incubating NOX with methacrylate beads lacking the aldehydes. As expected, 77%% of the offered protein was bound to the carrier after 20 hours. At this point, we decided to modify the immobilization media to avoid such hydrophobic interactions. To that aim, we added 30% of ethanol to reduce the polarity of the media and preclude the unspecific adsorption of NOX on the acrylic carrier PU-G. Pleasantly, we observed that the combination of ethanol and NH_2OH slowed down the immobilization of NOX on PU-G (Figure 1b), suggesting that now the immobilization was driven by the aldehyde chemistry rather than by the hydrophobic interactions. The slower immobilization promoted the

infiltration of NOX to the inner surface of PU-G (Figure 2b). These results agree with previous data reported for the lipase immobilization in presence of ethanol, which decreases the enzyme immobilization rate.[39] Thus, reducing the protein immobilization rate on the more hydrophobic acrylic-based carriers required two different immobilization competitors to obtain uniform protein distributions across the material microstructure. Hence, we demonstrate that the spatial organization of protein on these carriers must be controlled targeting two different immobilization mechanisms: aldehyde covalent chemistry and hydrophobic adsorption.

The activity of the immobilized NOX with different spatial distributions was assessed by standard colorimetric assay where air saturated buffer and low concentration of NADH were used. The spatial distribution of NOX across porous carriers affected enzyme recovered activity upon the immobilization process (Table 1). The specific activity of immobilized NOX ranged 17-55% of its soluble counterpart depending on the material type and the enzyme spatial organization. When NOX is located at the outer surface of agarose and acrylic materials, the resulting heterogeneous biocatalysts were 3 and 1.4 times more active, respectively, than when the enzyme was uniformly distributed towards them. Table 1 also shows that NOX non-uniformly immobilized on agarose carriers outperforms the same enzyme immobilized on acrylic ones. A plausible explanation for such a difference is that the hydrophilic nature of agarose beads may either prevent negative structural enzyme rearrangements or benefit the mass transport of the substrates[10–12], compared to the more hydrophobic methacrylate resin.

Table 1. Immobilization parameters of different preparation of NOX immobilized on different carriers activated with glyoxyl groups

Carrier material	Intraparticle protein distribution	Protein load (mg/g carrier)	Immobilization yield (%)	Specific activity (U/mg)	Relative recovered activity (%)
Agarose (AG-G)	Not uniform (Outer surface)	1	100	5.66	55
	Uniform	0.9	90	1.88	18
Methacrylate (PU-G)	Not uniform (Outer surface)	1	100	2.43	24
	Uniform	0.9	89	1.70	17

Reaction conditions: air saturated 25 mM sodium phosphate buffer pH 7.0, 25 °C, 0.15 mM FAD and 0.2 mM NADH under orbital shaking. Specific activity of soluble NOX = 10.2 U/mg

We hypothesize that the differences found in specific activity for the two enzyme distributions might be explained by a different level of the substrate restrictions towards the resulting heterogeneous biocatalyst. In order to elucidate the influence of spatial distribution on the substrate restrictions, and further mitigating them by the design of the enzyme-surface interface, we performed a series of experimental analysis tuning different variables such as enzyme loading and mixing condition.

Interrogating the measurable activity of immobilized NOX with different spatial organizations. The assay conditions for immobilized NOX significantly influence the results of its measurable activity, since it relies on two limiting substrates (oxygen and NADH) that need to be transferred from the liquid and liquid/gas interphase (reaction bulk) to solid phase (the biocatalyst). We study the enzyme activity using different biocatalysts and analysis conditions to elicit the limiting factors for the substrate mass transfer restrictions. To do so, NOX immobilized on both AG-G and PU-G with different loads and spatial distributions were measured under different mixing conditions (Figure 3 and S2).

Our first observation is that the specific activity increased under magnetic stirring for all the preparations, but with significant differences among the carriers and the protein spatial distributions (Figure 3 and S2). Expectedly, the better mixing conditions (magnetic stirring) results in more active heterogeneous biocatalysts, which is explained by the enhancement of the external mass transfer coefficients. This effect was more noticeable in AG-G carriers where the specific activity of the immobilized enzyme under magnetic stirring was roughly 10 times larger than under orbital shaking (Figure S2). Secondly, we find out that the specific activity of the immobilized enzyme significantly decreases at high protein loads, but it is highly influenced by both enzyme distribution and mixing conditions. The decrease of the apparent specific activity of the immobilized enzyme upon the increase of the loading is usually reasoned as being caused by substrates mass transfer restrictions, since the increase of substrate consumption rate eventually surpass the supply rate of substrate towards the enzyme.[15,21,33]

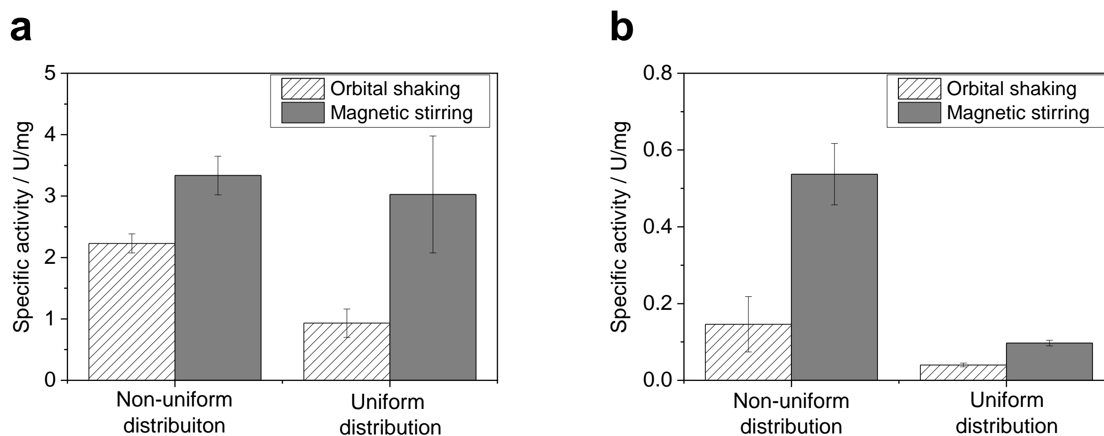

Figure 3. Effect of the mixing on the apparent activity of the immobilized NOX on PU-G at loading of (a) 0.1 mg/g and (b) 3 mg/g. Reaction conditions: 0.2 mM NADH, 0.15 mM FAD at 25 °C in 25 mM sodium phosphate buffer pH 7.0.

For low loadings (0.1 mg/g), the effect of the spatial distribution on the NOX activity only occurred under orbital shaking where the external diffusion restrictions are more dramatic (Figure 3a). We corroborate how the uniform distributions suffer a more aggravated substrate limitation, probably due to the thicker enzyme shell (a longer diffusional distance) through which the limiting substrate must diffuse. On the contrary, when external mass transfer resistances are erased (magnetic stirring) for low loading biocatalysts, uniform and non-uniform heterogeneous biocatalysts presented similar high specific activity regardless the enzyme spatial distribution.

For high loadings (3 mg/g), the biocatalysts were significantly less active than low loaded biocatalysts, regardless the mixing conditions and the enzyme spatial distribution (Figure 3b). A higher activity was observed under magnetic stirring conditions, but the non-uniform distribution now overpowered the uniform distribution under all the conditions. Unlike low loadings, the spatial distribution of NOX affected more significantly the specific activity of NOX immobilized on PU-G under magnetic stirring than under orbital shaking. Remarkably, immobilized NOX exhibited a specific activity of 0.097 and 0.54 U/mg under magnetic stirring, when the enzyme was uniformly and non-uniformly distributed within the carrier, respectively. Therefore, the control of the protein spatial organization permits to increase up to 5.5 times the activity of highly loaded heterogeneous biocatalysts under magnetic stirring conditions, yet specific activity is 19 times lower than the free enzyme (10.2 U/mg).

Hence, the optimal mixing conditions and the most suitable spatial distribution were insufficient to overcome the substrates (both oxygen and NADH) mass transport restrictions posed by the high immobilized enzyme loads. In this scenario, internal diffusional restrictions may limit the apparent activity, specially the one of the uniformly distributed enzymes,[33,40] as described for several hydrolases.[41,42] To assign the magnitude of the influence of NADH and O_2 limitations, and design strategies for their further mitigation, we studied the kinetics of oxygen time consumption courses provided by different NOX immobilized preparations.

Deciphering the influence of oxygen internal diffusional limitations and mitigation by the spatial organization of the immobilized NOX. To identify the internal diffusional limitations of O_2, we study O_2 consumption courses during the oxidation of NADH catalyzed by different preparations of immobilized NOX. To visualize the intraparticle oxygen gradient we have monitored O_2 concentration both in the liquid bulk and inside the particles following established

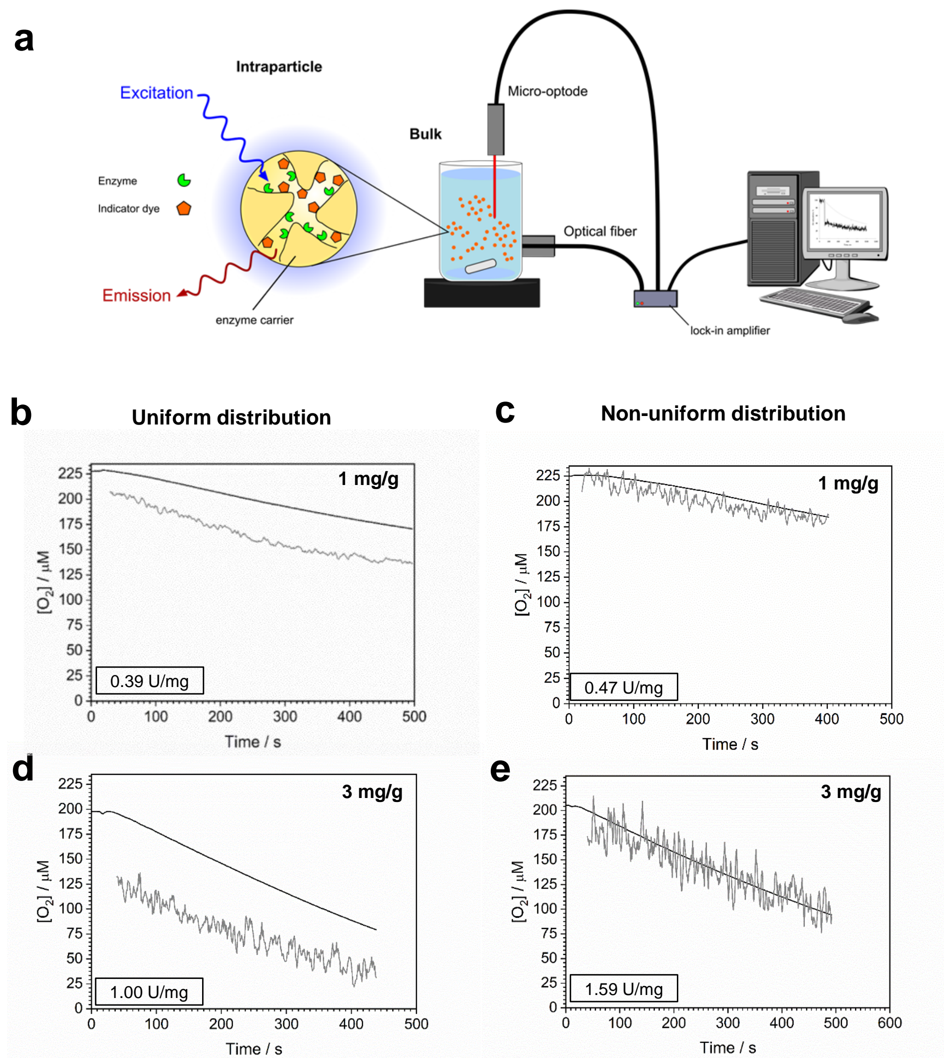

Figure 4. Oxygen time courses during the NADH oxidation catalyzed by different preparations of immobilized NOX. (a) Scheme of the principle of opto-chemical oxygen sensing in immobilized enzymes. Measurement of the space-averaged time-resolved internal O_2 concentration is based on the preparation of O_2-sensitive carrier material. The reading of the internal O_2 was carried out by a contactless measurement with fiber optic integrated with a phase modulation oxygen-meter, (details can be found in the SI). The scheme was adapted with permission from[33] Copyright 2020 John Wiley and Sons. (b-e) Time courses of the average intraparticle oxygen concentration (grey line) and the corresponding oxygen concentration in bulk (black line) when O_2 is utilized as substrate by an immobilized NOX. The enzyme distribution, the protein loading (mg/g) and the measured activity (U/g) of each biocatalyst are depicted in the graphs. Measurements were performed at 37 ºC, 12 µM FAD and 2 mM NADH.

procedures (Figure 4a).[5,34] The O_2 concentration in the liquid bulk was monitored by a commercial oxygen microoptode, whereas the internal O_2 concentration was quantified by opto-chemical sensing enabled by the co-immobilization of an O_2-sensitive luminescence dye with the enzyme inside the particles. PU-G carriers were used for immobilization and further O_2-sensing, since this type of materials are easily functionalized with the luminesce O_2-sensors through hydrophobic interactions.[5] Unfortunately, the hydrophilic nature of AG-G made unfeasible the integration of such luminophore within the porous structure to measure the intraparticle O_2 concentration.

Measurements were performed for heterogeneous biocatalysts differing in enzyme distribution, enzyme loading and using different NADH concentrations. When low-loaded (0.1 mg/g) immobilized NOX was used, the time courses of internal and external oxygen were superimposable (results not shown). Hence, oxygen gradients were not detected in accordance with the high recovered activity of low loaded heterogeneous biocatalysts measured under magnetic stirring, since oxygen diffusional limitations are unexpected to occur in this context. [33]

Same results were obtained when low concentration of NADH (<0.5 mM) were used regardless the biocatalyst loading. To focus on the oxygen limitations, we increased the NADH concentration up to an apparent saturating concentration (2 mM). Figure 4 b-e shows a set of exemplary results of the time courses of the oxygen consumption at saturating concentration of NADH using different immobilized and labelled biocatalysts. Here, we observed significant differences depending on the spatial organization of the immobilized NOX when high loads (> 1 mg/g) are used. Heterogeneous biocatalysts with uniform distributions show an oxygen gradient between bulk and intraparticle conditions (Figure 4b and d), indicating that the space-averaged oxygen concentration available for the enzyme within the carrier is remarkably lower than in the bulk. On the contrary, we observed no detectable difference between the external and internal oxygen concentration when using the non-uniformly distributed heterogeneous biocatalyst, demonstrating that enzyme location enables to reach a higher local oxygen concentration (Figure 4c and 4e). In fact, the higher activity determined from the bulk time-course oxygen consumption corroborates these results. Measurement of the available O_2 concentration inside solid carriers provided direct evidences on the occurrence of diffusional restrictions undergone by O_2-dependent immobilized enzymes.[33,35,36] In the literature, we find that enzyme loading and particle size critically influence the diffusional limitations and hence the measurable specific activity of the immobilized

enzyme.[40,41,43] Herein we show, for the first time, how the oxidase localization into the external shells of the particle is also a key parameter to minimize the oxygen gradient and therefore minimizing the limitations of the oxygen supply to the immobilized enzyme. Once we minimized the O_2 internal diffusional limitations, we focus on deciphering the influence of the NADH concentration.

Deciphering the influence of NADH concentration on the performance of immobilized NOX. The dependency of the activity upon NADH concentration was measured in absence of external mass transfer resistances under optimal mixing conditions for the catalysts with non-uniform distribution. To inquire in the internal mass transport restrictions suffered by the immobilized NOX at different protein loads, we quantified their initial reaction rates by monitoring the oxygen consumption at different NADH concentration. To this aim, we performed the oxidation reaction using NOX immobilized at the outer surface (non-uniform distribution) of PU-G under magnetic stirring. Figure 5 shows the specific activity of the immobilized NOX at different NADH concentrations (see also Figure S3 for the same representation in measurable activity; U/g carrier).

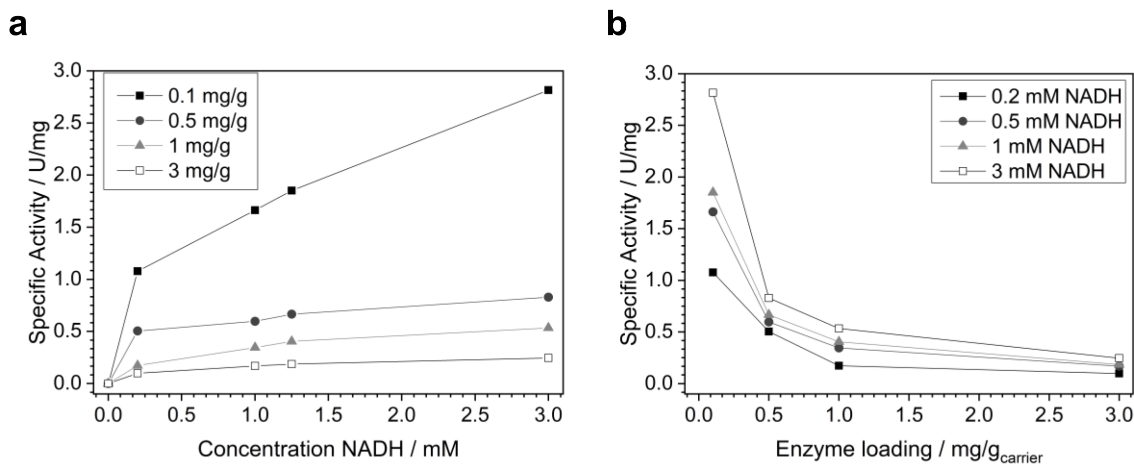

Figure 5. Specific activity of the NOX immobilized with non-uniform distribution at different enzyme loadings regarding to (a) the concentration of NADH and (b) the protein load. NOX immobilized on PU-G through a non-uniform distribution and operated under magnetic stirring. Reaction conditions: 0.2-3 mM NADH, 0.15 mM FAD at 25 °C in 25 mM sodium phosphate buffer pH 7.0.

The activities of all immobilized biocatalysts increase with the NADH concentration, which indicates that all the measurements performed at standard conditions (0.2 mM NADH, air saturated) are already dramatically limited by the cofactor available in the bulk. Especially, the specific activity of the biocatalyst with the lowest loading is significantly sensitive to the NADH concentration. At 3 mM of NADH, the recovered activity of the low loading reaches 30% of the corresponding for the free enzyme. As expected, the heterogeneous biocatalysts with higher loads displays lower specific activity under all NADH concentrations herein tested. Even at high apparently saturating concentration of NADH and non-uniform distribution measured under optimal mixing conditions, the specific activity is still below 5 % of the free enzyme. Given the high dependency of the activity on the cofactor concentration and the low specific activity detected for high enzyme loads, it is critical to implement a biocatalyst design that allows an efficient management of the cofactor transport without the need of high unfeasible external supply of NADH. This is especially important, not only due to the precious value of the NADH but also because the NOX is conceived to serve as cofactor-regenerating enzyme in redox biocascades, where the external concentration of NADH tends to be minimized.[44]

Co-immobilization of NOX and NADH to reduce the substrate internal diffusion restrictions underlying the heterogeneous biocatalysts. Suitable mixing conditions (magnetic stirring) minimize external mass transfer restriction of both oxygen and NADH, while the localization of NOX at the outermost regions of the porous carriers mitigates the internal oxygen diffusion restrictions. However, we still face some internal transport issues for the NADH, overall using more hydrophobic porous materials like PU-G. Under high NADH concentration in the bulk (3 mM), NOX non-uniformly immobilized on PU-G and AG-G with 1 mg/g load expressed a specific activity of 0.4 and 7.4 U/mg, respectively. These values mean the 4% and 73 % of the free enzyme specific activity (10.2 U/mg) under the same assay conditions. This is cumbersome to achieve highly active heterogeneous biocatalysts since intraparticle NADH gradients seem to jeopardize the activity of the immobilized NOX. To overcome this issue, we propose co-immobilizing NOX and NADH within the same porous particle to saturate the enzyme surroundings with its corresponding substrate and, consequently minimize NADH internal gradients. To that aim, we coated immobilized NOX non-uniformly distributed with polyethyleneimine (PEI) to make a cationic layer that reversibly binds NADH through its negatively charged phosphate groups (Figure 6a). We have recently exploited this proceeding to

ionically adsorb phosphorylated cofactors in the microenvironments of cofactor-dependent enzymes.[45–47] Such electrostatic interactions between the cofactor and the carrier porous structure establish an association/dissociation equilibrium that allows cofactor molecules to reach the NOX

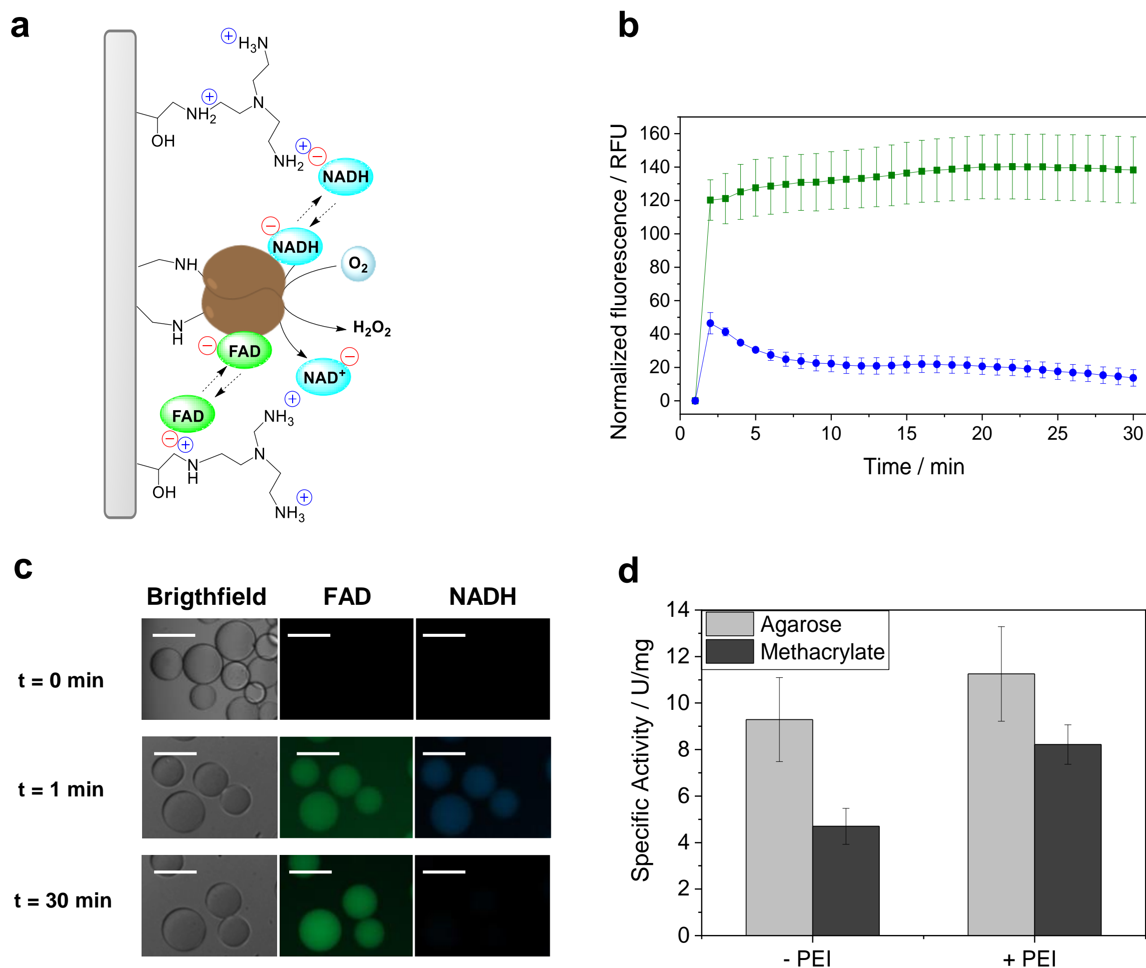

Figure 6. Analysis of cofactor co-immobilization. (a) Scheme of NOX (brown) and cofactors co-immobilization on AG-G coated with PEI. (b) Single-particle immobilization course of FAD (green) and NADH (blue) on AG-G immobilizing NOX and coated with PEI. (c) Epifluorescence microscopy images at different times recording brightfield, the autofluorescence of both FAD (green) and NADH (blue). White scale bars correspond to 100 µm. (d) Effect of cofactor co-immobilization on the recovered specific activity of the heterogeneous biocatalyst (1mg/g) using two different carriers under magnetic stirring, AG-G (light grey) and PU-G (dark grey).

active sites within the intraporal space. Since NOX activity also demands sub-stoichiometric amounts of flavin cofactors (FAD) as redox mediator to transfer the electron from NADH to the oxygen,[28,48] we also intended mitigating the mass transport restrictions potentially undergone by FAD. Our hypothesis is that the co-immobilization of FAD and NADH in the surrounding of the immobilized enzymes may enhance the effectiveness of the heterogeneous biocatalyst. Increasing the FAD concentration in the bulk has proven to increase the activity of soluble NOX.[28] Expectedly, NADH is ionically absorbed to agarose microbeads coated with PEI with a $K_d = 46 \pm 6$ µmol x g^{-1} according to its Langmuir isotherm (Figure S4). Besides, we also confirmed that FAD was reversibly bound to the PEI layer. According to its Langmuir isotherm, FAD presented a K_d (13 ± 1 µmol x g^{-1}) 3.5 times lower than the NADH although both phosphorylated cofactors reached similar maximum loadings, roughly 200 µmol x g^{-1}. This means that FAD is bound stronger than NADH to the carrier, but still reversible enough to reach the active sites of the immobilized NOX.

Next, we studied the kinetics of the immobilization of both phosphorylated cofactors through single-particle analysis, where the bindings of both NADH and FAD were monitored by reading their autofluorescence under an epifluorescence microscope. In both cases, quantitative cofactor adsorption was accomplished in less than 1 minute (Figure S5-S7), and they were uniformly distributed across the surface of the agarose microbeads, unlike NOX that was mostly located at the outer regions of the particles according to confocal laser scanning microscopy images (Figure S8). Such uniform spatial distribution coincides with the distributions found for other phosphorylated cofactors (NADPH and PLP) immobilized on other cationic porous carriers.[46,47] When both NADH and FAD were mixed with the heterogeneous biocatalyst coated with PEI, we observed an extremely fast decay of the NADH autofluorescence within the porous particles (Figure 6b) as consequence of the NADH oxidation to NAD^+ (lower autofluorescence) catalyzed by the immobilized NOX in presence of FAD. The fast immobilization of NADH precluded simultaneously monitoring the complete immobilization and the reaction time-course, yet the single-particle studies allowed *in operando* visualization of the confined reaction where NOX uses FAD to oxidize NADH (Figure 6c). Single-particle studies evidence that the NADH, and FAD, as soon as they are in contact with the reaction mixture, they are absorbed into the porous materials where NOX is immobilized and the oxidative reaction instantaneously occurs.

The cationic coating thus enables the concentration of both NADH and FAD in the surroundings of the immobilized enzymes. Figure 6d compares the recovered specific activity of NOX non-uniformly immobilized and coated with PEI at 1mg/g protein loads on two different carriers; AG-G and PU-G, under magnetic stirring. The presence of PEI increases 22 and 200 % the activity of NOX immobilized on AG-G and PU-G, respectively, since the solid-phase now concentrates both NADH and FAD in the surroundings of enzyme. The 38% lower apparent K_M values towards NADH when the immobilized NOX was coated with PEI (Figure S9) support that effective NADH concentration (substrate) within the porous beads is higher than in the bulk, which enhances the specific activity of the immobilized NOX. In fact, the apparent k_{cat} of NOX immobilized on AG-G increases roughly two times when coated with PEI, regardless the protein distribution, reaching a similar value to the one previously reported for the soluble enzyme.[28] The saturation of NOX surroundings with NADH and FAD was remarkably beneficial when the enzyme was immobilized on PU-G, since the cationic PEI layer now overcomes the NADH external diffusion restrictions posed by the hydrophobic nature of this acrylic carrier. We also studied the effect of NADH co-immobilization on the H_2O_2 production rate that provides information about the second step of NOX reaction where the reduced flavin transfers the electron to oxygen as final acceptor. To this aim, we coupled a NADH-compatible colorimetric peroxidase assay to quantify both the consumed NADH and the formed H_2O_2. We converge into the same result; the co-immobilization of NADH and NOX on agarose carriers increases its specific activity (Figure S10).

Figure 7 summarizes all technological efforts done to increase the NOX activity along the different engineering stages. Through this optimization trip, we have ramped up the apparent specific activity value of immobilized NOX 6.5-fold, through selecting the hydrophilic carriers like agarose, locating the enzymes a the outer surface of the microbeads carriers, operating the heterogeneous biocatalyst under optimal mixing conditions (magnetic stirring) and confining both enzymes and substrates within the same carrier particle. This outstanding activity enhancement was possible through mitigating both oxygen and NADH mass transfer restrictions, giving rise an immobilized NOX whose apparent specific activity is 11±2 U/mg; an effectiveness of roughly 100% compared with the free NOX measured under the same aeration, temperature and pH conditions and using the same substrate concentrations.

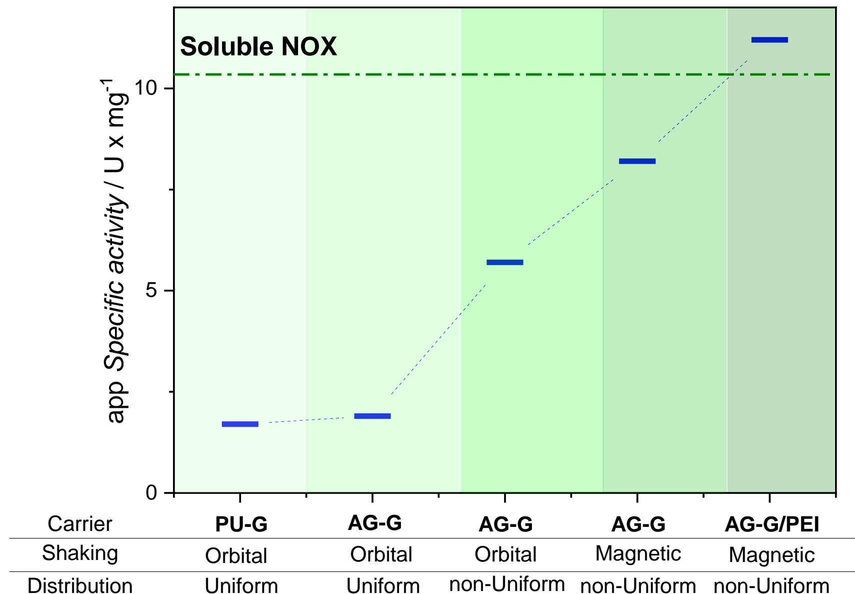

Figure 7. Engineering path to enhance the apparent specific activity of immobilized NOX. Reaction conditions for all measurements: 0.2 mM NADH, 0.15 mM FAD at 25 °C in 25 mM sodium phosphate buffer pH 7.0. The load of the immobilized enzymes was 1 mg x g^{-1} in all cases.

CONCLUSIONS

The optimization of heterogeneous biocatalysts based on cofactor and oxygen dependent oxidoreductases is not trivial. Herein, we have optimized the immobilization of NOX from a thermophilic organism on porous carriers to mitigate those substrate mass transport issues that limit the catalytic performance of an immobilized biocatalyst. We firstly engineered the spatial distribution of NOX across the porous surface using two different carriers based on agarose and acrylic materials. We found that the outer localization of the enzyme improves the effective supply of oxygen, enhancing the specific activity of the biocatalysts. Then we studied the effect of the mixing conditions on the enzyme activity. The more efficient mixing conditions (provided by stirring magnetic bars) are reflecting in the higher activity of the immobilized enzyme. Finally, to overcome the NADH transport limitation, we co-immobilized the enzyme with the substrate; NADH, and its redox mediator; FAD. This heterogeneous biocatalyst only needed the exogenous supply of the molecular oxygen to work, therefore under optimal O_2 supply, its apparent catalytic

efficiency scaled up to its maximum value. This study exemplifies the critical design and characterization aspects to control the spatiotemporal gradients occurring inside the heterogeneous biocatalysts, thus maximizing catalyst productivity. This was possible through a multi-scale control of the interactions between the enzyme, the substrates and the carriers rather than using carriers with different dimensions. Therefore, we herein deploy a set of state-of-the-art characterization techniques that merge conventional bulk steady-state experiments and intraparticle microscopic measurements to guide us during the preparation more efficient and robust heterogeneous biocatalysts.

EXPERIMENTAL SECTION

Materials. Flavine adenine dinucleotide oxidized form (FAD), hydroxylamine, ethanolamine, peroxidase from horseradish, polyethyleneimine 25 kDa (PEI25), Amplifluᵀᴹ Red, ampicillin and IPTG were acquired from Sigma-Aldrich (St. Louis, IL). Nicotinamide adenine dinucleotide reduced sodium salt (NADH) was purchased from GERBU Biotechnik GmbH (Wieblingen, Germany). Plain agarose microbeads were purchased from ABT technologies (Madrid, Spain) to fabricate glyoxyl-agarose. Tris(4,7-diphenyl-1,10-phenanthroline) ruthenium (II) dichlorire ($Ru(dpp)_3$) was purchased from ABCR GmbH. Lifetech Purolite ECR 8215F was kindly donated by Purolite Ltd. (Llantrisant, U.K.). Inc. 8-well µslides were supplied by Ibidi (Planegg, Germany). All other reagents and solvents were of analytical grade or superior.

Protein expression and purification. NOX was overexpressed in *E. coli* as follows[49]. Briefly, 1 mL of an overnight culture of *E. coli* BL21-Gold transformed with the respective plasmid (*nox*_pET22a) was inoculated in a 50 mL of LB medium containing ampicillin (100 µg/mL). The culture was incubated at 37 °C and 200 rpm until the OD_{600nm} reached 0.6. At that point, the culture was induced with 1 mM IPTG. Cells were grown at 37 °C for 3 hours and then harvested by centrifugation at 4000 g during 30 minutes at 4 ºC. The resulting pellet was resuspended in 5 mL of 25 mM sodium phosphate at pH 7. Cells were broken by sonication (LABSONIC P, Sartorius Stedim biotech) at 30% of amplitude (5 sec ON, 5 sec OFF) during 30 minutes. The suspension was centrifuged at 10000 g during 30 minutes at 4 ºC. The supernatant was incubated at 80 ºC during 45 minutes. The protein solution was then centrifugated at 10000 g

during 30 minutes at 4 ºC to separate NOX in the supernatant. The purification process of NOX was checked by SDS-PAGE (Figure S11).

Protein quantification. Bradford protein assay[50] was adapted to 96-well plates. Briefly, 5 µL of enzyme solution were mixed with 200 µL of Bradford reagent and incubated at room temperature for 5 min. Then, the absorbance was measured at 595 nm and the protein content was estimated employing a calibration curve using BSA as a standard.

Enzymatic activity assay. One unit of activity was defined as the amount of enzyme needed to oxidize 1 µmol of NADH at 25 ºC. The decrease in the absorbance was spectrophotometrically monitored at 340 nm. Two measurement formats were employed;

Well-plate: 200 µL of 0.15 mM FAD and 0.2-2 mM NADH in 25 mM sodium phosphate buffer at pH 7 were incubated with 10 µL of enzymatic solution or suspension in a 96-well plate under orbital shaking.

Cuvette: 1.5 – 2 mL of 0.15 mM FAD and 0.2-2 mM NADH in 25 mM sodium phosphate buffer at pH 7 were incubated with 10 µL of enzymatic solution or suspension in a cuvette under magnetic stirring.

Activation of supports. Glyoxyl-agarose (AG-G) and glyoxyl-Purolite (Pu-G) were prepared as described elsewhere.[51] Briefly, 1 g of either epoxy-agarose or epoxy-methacrylate was incubated with 10 mL of 100 mM H_2SO_4 overnight and under orbital shaking. Then, the resin was filtered and washed 10 times with 10 volumes of water. To oxidize the resulting glyceryl-support, 10 mL of 30 mM $NaIO_4$ were added and the suspension was incubated for 2 h under orbital shaking. Finally, the glyoxyl-support was washed 10 times with 10 volumes of water and stored at 4 ºC until use.

Immobilization of NOX on glyoxyl-activated carriers. 10 mL of NOX (0.01 - 0.3 mg/mL) in 100 mM sodium bicarbonate buffer at pH 10 were mixed with 1 g of AG-G and incubated at room temperature under orbital shaking for 3 hours. Immobilization course was followed spectrophotometrically by measuring the activity of both suspension and supernatant. To slow down the immobilization process of NOX on agarose, 10 mM hydroxylamine was added to the suspension. In case of immobilization on methacrylate, 10 mM hydroxylamine and 154 mM ethanol were added to slow down the immobilization.

PEI-coating of NOX immobilized on agarose and methacrylate carriers .When PEI-coating was applied after enzyme immobilization, 1 g of AG-G was mixed with 10 mL of a 10

mg/mL PEI solution in 100 mM bicarbonate buffer solution at pH 10 under orbital shaking for 1 hour at 25 ºC. Later on, solid $NaBH_4$ was added (final concentration 1 mg/mL) and incubated for 30 min at 4 ºC. Finally, the AG-G/PEI25 was washed 5 times with 10 volumes of water and stored at 4 ºC.

Cofactor co-immobilization. After PEI-coating, ionic adsorption of NADH was achieved by incubating 10 mL of 1 mM NADH solution in 10 mM sodium phosphate at pH 7 with 1 gram of agarose microbeads with previously immobilized enzymes. The suspension was kept under orbital shaking for 1 hour at room temperature. Afterwards, the resin was filtered and washed three times with 1 mL of 10 mM sodium phosphate at pH 7. The immobilization yield of NADH was calculated by measuring the absorbance of the supernatant after the adsorption process and after each washing step at 340 nm in the well-plate reader.[45]

NOX activity through monitoring H_2O_2 production. 200 µL of a reaction mixture containing 0.2 mM NADH, 0.15 mM FAD, 0.05 mM Ampliflu™ Red and 25 µg/mL HRP in 25 mM sodium phosphate buffer at pH 7 were added to the immobilized biocatalyst. NOX immobilized on agarose (1 mg/g), the same biocatalyst coated with PEI and another preparation coated with PEI and with co-immobilized NADH were used as immobilized biocatalysts. NADH and H_2O_2 production were simultaneously monitored at 340 nm and 520 nm, respectively, at 25°C for 15 minutes in the well-plate reader.

Intraparticle protein distribution analysis by fluorescence CLSM. 20 mg of the immobilized biocatalysts were added to 200 µL of buffer solution in an 8-well µslide. In case of methacrylate carrier, the buffer solution contained 50% glycerol to improve the match in refractive index between the medium and the opaque beads. Since the intrinsic FAD of the enzyme exhibits autofluorescence, the spatial distribution of the enzyme across the carrier was analyzed using a ZEISS confocal microscope LSM880 with λ_{ex}: 488 nm and λ_{ex}: 520 nm. Images were processed with the software FIJI using a LUT (Yellow hot).

Opto-chemical O_2 sensing in bulk solution and inside the solid support. The O_2 concentration in bulk solution was measured using a fiber-optic oxygen microoptode (Optical Oxygen Meter – FireStingO_2). 100 µL of a suspension of 1:10 (w/v) immobilized NOX on PU-G (0.1 mg/g, 0.5 mg/g, 1 mg/g, and 3 mg/g) were added to 4 mL of substrate solution containing NADH (0.2 mM, 1 mM, 1.25 mM and 3 mM) and 0.025 mM FAD in air-saturated 25 mM sodium phosphate buffer at pH 7 in an open glass vial (1.2 cm diameter). The set up took place at 25°C

and 300 rpm magnetic stirring (6 x 3 mm) as described before.[4,5] For the intra-particle O_2 sensing, two immobilized biocatalysts on PU-G with different protein loadings (0.1 mg/g and 3 mg/g) were labeled with $Ru(dpp)_3$ (25% of 5 g/L $Ru(dpp)_3$ in ethanol) in air-saturated 25 mM sodium phosphate buffer pH 7 at 30ºC. The $Ru(dpp)_3$ load was 5 mg/g. The suspension was incubated for 10 minutes at room temperature under orbital shaking. The excess of $Ru(dpp)_3$ was washed out with the same buffer till the supernatant was clear. 200 µL of a suspension of 1:10 (w/v) immobilized NOX were added to 4 mL of a substrate solution containing NADH (0.2 mM and 3 mM) and 0.025 mM FAD in air-saturated 25 mM sodium phosphate buffer at pH 7. The oxygen consumption was monitored as described elsewhere[4] (see supporting methodology for more details).

Supporting Information.

Supporting methodology. Influence of protein loading, mixing method and enzyme distribution on the performance of the immobilized biocatalyst (Figures S1-S3). Langmuir isotherms for the ionic adsorption of NADH to different beads coated with PEI (Figure S4). CLSM micrographs for the immobilization of FAD and NAD+ (Figures S5-S8). Michaelis-Menten plots of NOX immobilized with and without PEI and the effect of the cofactor co-immobilization on the activity of the immobilized NOX (Figure S9-S10). Expression and purification of NOX (Figures S11)

AUTHOR INFORMATION

Corresponding Authors

* F. López-Gallego: flopez@cicbiomagune.es

* J. M. Bolivar: juanmbol@ucm.es

Author contributions

Experiments were performed by ABM and CH. The manuscript was written by JMB and FLG.

The work was conceptualized by JMB and FLG. Funding was secured by BN, JMB and FLG.

All authors discussed the results and revised the manuscript. All authors have given approval to the final version of the present manuscript.

Notes

The authors declare no competing financial interest.

ACKNOWLEDGMENTS

A.I.B.-M and F.L.-G. are grateful to MINECO (RTI2018-094398-B-I00). ERC-Co (METACELL-878089)) and ERA-CoBioTech (Project ID: 61 HOMBIOCAT/ PCI2018-092984) projects are acknowledged for funding F.L-G. F.L-G. also thanks IKERBASQUE foundation. C.H. acknowledges ERASMUS+ for the student exchange grant from the University of Graz to the University of Zaragoza. J.M.B. acknowledges funding from the Government of Community of Madrid (2018-T1/BIO-10200). The authors are grateful to Purolite® for the kind donation of resins.

ABBREVIATIONS

AG-G, agarose microbeads activated with glyoxyl groups; AG-G/PEI25, agarose microbeads activated with glyoxyl groups and coated with polyethyleneimine 25 kDa; CLSM, confocal laser scanning microscopy; FAD, Flavin adenine dinucleotide; HRP, peroxidase from horseradish; IPTG, isopropyl-β-D-1-thiogalactopyranoside; K_d, dissociation constant; LUT, look-up table for color grading; NAD(H), nicotinamide adenine dinucleotide; NADP(H), nicotinamide adenine dinucleotide phosphate; NOX, NAD(P)H flavin-oxidases; PEI, polyethyleneimine; PU-G, Purolite ECR8215F (methacrylate) microbeads activated with glyoxyl groups; ROI, region of interest.

REFERENCES

(1) Sheldon, R. A.; van Pelt, S. Enzyme Immobilisation in Biocatalysis: Why, What and How. *Chem. Soc. Rev.* **2013**, *42* (15), 6223–6235. https://doi.org/10.1039/C3CS60075K.

(2) Thompson, M. P.; Peñafiel, I.; Cosgrove, S. C.; Turner, N. J. Biocatalysis Using Immobilized Enzymes in Continuous Flow for the Synthesis of Fine Chemicals. *Org. Process Res. and Dev*. **2019**, 9–18. https://doi.org/10.1021/acs.oprd.8b00305.

(3) Buurmans, I. L. C.; Weckhuysen, B. M. Heterogeneities of Individual Catalyst Particles in Space and Time as Monitored by Spectroscopy. *Nat. Chem.* **2012**, 873–886. https://doi.org/10.1038/nchem.1478.

(4) Bolivar, J. M.; Eisl, I.; Nidetzky, B. Advanced Characterization of Immobilized Enzymes as Heterogeneous Biocatalysts. *Catal. Today* **2016**, *259*, 66–80. https://doi.org/10.1016/j.cattod.2015.05.004.

(5) Bolivar, J. M.; Nidetzky, B. The Microenvironment in Immobilized Enzymes: Methods of Characterization and Its Role in Determining Enzyme Performance. *Molecules* **2019**, *24* (19) 3460. https://doi.org/10.3390/molecules24193460.

(6) Hanefeld, U.; Gardossi, L.; Magner, E. Understanding Enzyme Immobilisation. *Chem. Soc. Rev.* **2009**, *38* (2), 453–468. https://doi.org/10.1039/B711564B.

(7) Hoarau, M.; Badieyan, S.; Marsh, E. N. G. Immobilized Enzymes: Understanding Enzyme-Surface Interactions at the Molecular Level. *Org. Biomol. Chem.* **2017**, 9539–9551. https://doi.org/10.1039/c7ob01880k.

(8) Secundo, F. Conformational Changes of Enzymes upon Immobilisation. *Chem. Soc. Rev.* **2013**, *42* (15), 6250–6261. https://doi.org/10.1039/c3cs35495d.

(9) Bolivar, J. M.; Nidetzky, B. On the Relationship between Structure and Catalytic Effectiveness in Solid Surface-Immobilized Enzymes: Advances in Methodology and the Quest for a Single-Molecule Perspective. *Biochimica et Biophysica Acta - Proteins and Proteomics*. Elsevier B.V. **2020**. https://doi.org/10.1016/j.bbapap.2019.140333.

(10) Rodrigues, R. C.; Ortiz, C.; Berenguer-Murcia, Á.; Torres, R.; Fernández-Lafuente, R. Modifying Enzyme Activity and Selectivity by Immobilization. *Chem. Soc. Rev.* **2013**, *42* (15), 6290–6307. https://doi.org/10.1039/C2CS35231A.

(11) Sigurdardóttir, S. B.; Lehmann, J.; Ovtar, S.; Grivel, J.; Negra, M. Della; Kaiser, A.; Pinelo, M. Enzyme Immobilization on Inorganic Surfaces for Membrane Reactor Applications: Mass Transfer Challenges, Enzyme Leakage and Reuse of Materials. *Adv. Synth. Catal.* **2018**, *360* (14), 2578–2607. https://doi.org/10.1002/adsc.201800307.

(12) Liese, A.; Hilterhaus, L. Evaluation of Immobilized Enzymes for Industrial Applications. *Chem. Soc. Rev.* **2013**, *42* (15), 6236–6249. https://doi.org/10.1039/C3CS35511J.

(13) Volokitina, M. V.; Nikitina, A. V.; Tennikova, T. B.; Korzhikova-Vlakh, E. G. Immobilized Enzyme Reactors Based on Monoliths: Effect of Pore Size and Enzyme Loading on Biocatalytic Process. *Electrophoresis* **2017**, *38* (22–23), 2931–2939. https://doi.org/10.1002/elps.201700210.

(14) Cantone, S.; Ferrario, V.; Corici, L.; Ebert, C.; Fattor, D.; Spizzo, P.; Gardossi, L. Efficient Immobilisation of Industrial Biocatalysts: Criteria and Constraints for the Selection of

Organic Polymeric Carriers and Immobilisation Methods. *Chem. Soc. Rev.* **2013**, *42* (15), 6262–6276. https://doi.org/10.1039/c3cs35464d.

(15) Liese, A.; Hilterhaus, L. Evaluation of Immobilized Enzymes for Industrial Applications. *Chem. Soc. Rev.* **2013**, *42* (15), 6236–6249. https://doi.org/10.1039/c3cs35511j.

(16) Rocha-Martín, J.; Rivas, B. de las; Muñoz, R.; Guisán, J. M.; López-Gallego, F. Rational Co-Immobilization of Bi-Enzyme Cascades on Porous Supports and Their Applications in Bio-Redox Reactions with In Situ Recycling of Soluble Cofactors. *ChemCatChem* **2012**, *4* (9), 1279–1288. https://doi.org/10.1002/cctc.201200146.

(17) Ladero, M.; Santos, A.; Garcia-Ochoa, F. Hindered Diffusion of Proteins and Polymethacrylates in Controlled-Pore Glass: An Experimental Approach. *Chem. Eng. Sci.* **2007**, *62* (3), 666–678. https://doi.org/10.1016/j.ces.2006.09.040.

(18) Ladero, M.; Santos, A.; García-Ochoa, F. Diffusion and Chemical Reaction Rates with Nonuniform Enzyme Distribution: An Experimental Approach. *Biotechnol. Bioeng.* **2001**, *72* (4), 458–467. https://doi.org/10.1002/1097-0290(20000220)72:4<458::AID-BIT1007>3.0.CO;2-R.

(19) Do, D. D.; Clark, D. S.; Bailey, J. E. Modeling Enzyme Immobilization in Porous Solid Supports. *Biotechnol. Bioeng.* **1982**, *24* (7), 1527–1546. https://doi.org/10.1002/bit.260240707.

(20) Van Roon, J. L.; Joerink, M.; Rijkers, M. P. W. M.; Tramper, J.; P. H. Schroën, C. G.; Beeftink, H. H. Enzyme Distribution Derived from Macroscopic Particle Behavior of an Industrial Immobilized Penicillin-G Acylase. *Biotechnol. Prog.* **2003**, *19* (5), 1510–1518.

https://doi.org/10.1021/bp0340638.

(21) Borchert, A.; Buchholz, K. Improved Biocatalyst Effectiveness by Controlled Immobilization of Enzymes. *Biotechnol. Bioeng.* **1984**, *26* (7), 727–736. https://doi.org/10.1002/bit.260260715.

(22) Dennis, K. E.; Clark, D. S.; Bailey, J. E.; Cho, Y. K.; Park, Y. H. Immobilization of Enzymes in Porous Supports: Effects of Support–Enzyme Solution Contacting. *Biotechnol. Bioeng.* **1984**, *26* (8), 892–900. https://doi.org/10.1002/bit.260260812.

(23) Hossain, M. M.; Do, D. D. Determination of Intrinsic Parameters for Immobilization Reactions of Catalase and Amyloglucosidase in Porous Glass Supports. *Biotechnol. Bioeng.* **1988**, *31* (7), 730–736. https://doi.org/10.1002/bit.260310716.

(24) Bolivar, J. M.; Hidalgo, A.; Sánchez-Ruiloba, L.; Berenguer, J.; Guisán, J. M.; López-Gallego, F. Modulation of the Distribution of Small Proteins within Porous Matrixes by Smart-Control of the Immobilization Rate. *J. Biotechnol.* **2011**, *155* (4), 412–420. https://doi.org/https://doi.org/10.1016/j.jbiotec.2011.07.039.

(25) Benítez-Mateos, A. I.; Nidetzky, B.; Bolivar, J. M.; López-Gallego, F. Single-Particle Studies to Advance the Characterization of Heterogeneous Biocatalysts. *ChemCatChem* **2018**, *10* (4) 654. https://doi.org/10.1002/cctc.201701590.

(26) Rocha-Martin, J.; Acosta, A.; Guisan, J. M.; López-Gallego, F. Immobilizing Systems Biocatalysis for the Selective Oxidation of Glycerol Coupled to In Situ Cofactor Recycling and Hydrogen Peroxide Elimination. *ChemCatChem* **2015**, *7* (13), 1939–1947. https://doi.org/10.1002/cctc.201500210.

(27) Xu, M. Q.; Li, F. L.; Yu, W. Q.; Li, R. F.; Zhang, Y. W. Combined Cross-Linked Enzyme Aggregates of Glycerol Dehydrogenase and NADH Oxidase for High Efficiency in Situ NAD+ Regeneration. *Int. J. Biol. Macromol.* **2020**, *144*, 1013–1021. https://doi.org/10.1016/j.ijbiomac.2019.09.178.

(28) Rocha-Martín, J.; Vega, D.; Bolivar, J. M.; Godoy, C. A.; Hidalgo, A.; Berenguer, J.; Guisán, J. M.; López-Gallego, F. New Biotechnological Perspectives of a NADH Oxidase Variant from Thermus Thermophilus HB27 as NAD+-Recycling Enzyme. *BMC Biotechnol.* **2011**, *11* (1), 101. https://doi.org/10.1186/1472-6750-11-101.

(29) Rehn, G.; Pedersen, A. T.; Woodley, J. M. Application of NAD(P)H Oxidase for Cofactor Regeneration in Dehydrogenase Catalyzed Oxidations. *J. Mol. Catal. B Enzym.* **2016**, *134*, 331–339. https://doi.org/10.1016/j.molcatb.2016.09.016.

(30) Jiang, R.; Bommarius, A. S. Hydrogen Peroxide-Producing NADH Oxidase (Nox-1) from Lactococcus Lactis. *Tetrahedron Asymmetry* **2004**, *15* (18), 2939–2944. https://doi.org/10.1016/j.tetasy.2004.07.057.

(31) Sudar, M.; Findrik, Z.; Domanovac, M. V.; Vasić-Rački, D. Coenzyme Regeneration Catalyzed by NADH Oxidase from Lactococcus Lactis. *Biochem. Eng. J.* **2014**, *88*, 12–18. https://doi.org/10.1016/j.bej.2014.04.001.

(32) Jiang, R.; Riebel, B. R.; Bommarius, A. S. Comparison of Alkyl Hydroperoxide Reductase (AhpR) and Water-Forming NADH Oxidase from Lactococcus Lactis ATCC 19435. *Adv. Synth. Catal.* **2005**, *347* (7–8), 1139–1146. https://doi.org/10.1002/adsc.200505063.

(33) Bolivar, J. M.; Consolati, T.; Mayr, T.; Nidetzky, B. Quantitating Intraparticle O2 Gradients

in Solid Supported Enzyme Immobilizates: Experimental Determination of Their Role in Limiting the Catalytic Effectiveness of Immobilized Glucose Oxidase. *Biotechnol. Bioeng.* **2013**, *110* (8), 2086–2095. https://doi.org/10.1002/bit.24873.

(34) Bolivar, J. M.; Consolati, T.; Mayr, T.; Nidetzky, B. Shine a Light on Immobilized Enzymes: Real-Time Sensing in Solid Supported Biocatalysts. *Trends Biotechnol.* **2013**, *31* (3), 194–203. https://doi.org/https://doi.org/10.1016/j.tibtech.2013.01.004.

(35) Bolivar, J. M.; Schelch, S.; Mayr, T.; Nidetzky, B. Mesoporous Silica Materials Labeled for Optical Oxygen Sensing and Their Application to Development of a Silica-Supported Oxidoreductase Biocatalyst. *ACS Catal.* **2015**, *5* (10), 5984–5993. https://doi.org/10.1021/acscatal.5b01601.

(36) Bolivar, J. M.; Schelch, S.; Mayr, T.; Nidetzky, B. Dissecting Physical and Biochemical Factors of Catalytic Effectiveness in Immobilized D-Amino Acid Oxidase by Real-Time Sensing of O_2 Availability Inside Porous Carriers. *ChemCatChem* **2014**, *6* (4), 981–986. https://doi.org/10.1002/cctc.201301026.

(37) Rocha-Martin, J.; Sánchez-Murcia, P. A.; López-Gallego, F.; Hidalgo, A.; Berenguer, J.; Guisan, J. M. Functional Characterization and Structural Analysis of NADH Oxidase Mutants from Thermus Thermophilus HB27: Role of Residues 166, 174, and 194 in the Catalytic Properties and Thermostability. *Microorganisms* **2019**, *7* (11). https://doi.org/10.3390/microorganisms7110515.

(38) Jokerst, J. V.; Chou, J.; Camp, J. P.; Wong, J.; Lennart, A.; Pollard, A. A.; Floriano, P. N.; Christodoulides, N.; Simmons, G. W.; Zhou, Y.; Ali, M. F.; McDevitt, J. T. Location of

Biomarkers and Reagents within Agarose Beads of a Programmable Bio-Nano-Chip. *Small* **2011**, *7* (5), 613–624. https://doi.org/10.1002/smll.201002089.

(39) Barbosa, O.; Torres, R.; Ortiz, C.; Fernandez-Lafuente, R. The Slow-down of the CALB Immobilization Rate Permits to Control the Inter and Intra Molecular Modification Produced by Glutaraldehyde. *Process Biochem.* **2012**, *47* (5), 766–774. https://doi.org/10.1016/j.procbio.2012.02.009.

(40) Illanes, A.; González, J. M.; Gómez, J. M.; Valencia, P.; Wilson, L. Diffusional Restrictions in Glyoxyl-Agarose Immobilized Penicillin G Acylase of Different Particle Size and Protein Loading. *Electron. J. Biotechnol.* **2010**, *13* (1), 1–9. https://doi.org/10.2225/vol13-issue1-fulltext-12.

(41) Bahamondes, C.; Álvaro, G.; Wilson, L.; Illanes, A. Effect of Enzyme Load and Catalyst Particle Size on the Diffusional Restrictions in Reactions of Synthesis and Hydrolysis Catalyzed by α-Chymotrypsin Immobilized into Glyoxal-Agarose. *Process Biochem.* **2017**, *53*, 172–179. https://doi.org/10.1016/j.procbio.2016.12.004.

(42) Ladero, M.; Santos, A.; García-Ochoa, F. Diffusion and Chemical Reaction Rates with Nonuniform Enzyme Distribution: An Experimental Approach. *Biotechnol. Bioeng.* **2001**, *72* (4), 458–467. https://doi.org/10.1002/1097-0290(20000220)72:4<458::AID-BIT1007>3.0.CO;2-R.

(43) Valencia, P.; Flores, S.; Wilson, L.; Illanes, A. Effect of Particle Size Distribution on the Simulation of Immobilized Enzyme Reactor Performance. *Biochem. Eng. J.* **2010**, *49* (2), 256–263. https://doi.org/10.1016/j.bej.2010.01.002.

(44) Knaus, T.; Tseliou, V.; Humphreys, L. D.; Scrutton, N. S.; Mutti, F. G. A Biocatalytic Method for the Chemoselective Aerobic Oxidation of Aldehydes to Carboxylic Acids. *Green Chem.* **2018**, *20* (17), 3931–3943. https://doi.org/10.1039/c8gc01381k.

(45) Velasco-Lozano, S.; Benítez-Mateos, A. I.; López-Gallego, F. Co-Immobilized Phosphorylated Cofactors and Enzymes as Self-Sufficient Heterogeneous Biocatalysts for Chemical Processes. *Angew. Chem. Int. Ed.* **2017**, *56* (3) 771-775. https://doi.org/10.1002/anie.201609758.

(46) Benítez-Mateos, A. I.; San Sebastian, E.; Ríos-Lombardía, N.; Morís, F.; González-Sabín, J.; López-Gallego, F. Asymmetric Reduction of Prochiral Ketones by Using Self-Sufficient Heterogeneous Biocatalysts Based on NADPH-Dependent Ketoreductases. *Chem. Eur. J.* **2017**, *23* (66) 16843. https://doi.org/10.1002/chem.201703475.

(47) Benítez-Mateos, A. I.; Contente, M. L.; Velasco-Lozano, S.; Paradisi, F.; López-Gallego, F. Self-Sufficient Flow-Biocatalysis by Coimmobilization of Pyridoxal 5′-Phosphate and ω-Transaminases onto Porous Carriers. *ACS Sustain. Chem. Eng.* **2018**, *6* (10) 13151-13159. https://doi.org/10.1021/acssuschemeng.8b02672.

(48) Nowak, C.; Beer, B.; Pick, A.; Roth, T.; Lommes, P.; Sieber, V. A Water-Forming NADH Oxidase from Lactobacillus Pentosus Suitable for the Regeneration of Synthetic Biomimetic Cofactors. *Front. Microbiol.* **2015**, 957. https://doi.org/10.3389/fmicb.2015.00957.

(49) Rocha-Martin, J.; Vega, D. E.; Cabrera, Z.; Bolivar, J. M.; Fernandez-Lafuente, R.; Berenguer, J.; Guisan, J. M. Purification, Immobilization and Stabilization of a Highly

Enantioselective Alcohol Dehydrogenase from Thermus Thermophilus HB27 Cloned in E. Coli. *Process Biochem.* **2009**, *44* (9), 1004–1012. https://doi.org/10.1016/j.procbio.2009.04.026.

(50) Bradford, M. M. A Rapid and Sensitive Method for the Quantitation of Microgram Quantities of Protein Utilizing the Principle of Protein-Dye Binding. *Anal. Biochem.* **1976**, *72*, 248–254. https://doi.org/10.1016/0003-2697(76)90527-3.

(51) Mateo, C.; Bolivar, J. M.; Godoy, C. A.; Rocha-Martin, J.; Pessela, B. C.; Curiel, J. A.; Muñoz, R.; Guisan, J. M.; Fernández-Lorente, G. Improvement of Enzyme Properties with a Two-Step Immobilizaton Process on Novel Heterofunctional Supports. *Biomacromolecules* **2010**, *11* (11), 3112–3117. https://doi.org/10.1021/bm100916r.

Table of contents (TOC):